JOURNAL OF ENERGY SYSTEMS

VOLUME 2, ISSUE 3

2602-2052

DOI: 10.30521/jes.453560

Research Article

Piezo-actuated common rail injector structure and efficient design

Hasan Koten
Istanbul Medeniyet University, Istanbul, Turkey, hasan.koten@medeniyet.edu.tr, hasan.koten@brunel.ac.uk, ORCID: 0000-0002-1907-9420
Ebubekir Can Gunes
Istanbul Medeniyet University, Istanbul, Turkey, gunesebubekir@gmail.com, ORCID: 0000-0002-0060-2285
Kubilay Guner
AlbarakaTurk Co., Istanbul, Turkey, kubilay.guner@hotmail.com, ORCID: 0000-0002-2206-6276

Arrived: 14.08.2018 Accepted: 18.09.2018 Published: 30.09.2018

Abstract: Piezo-actuated common rail injectors are often utilized in today's automobile engines' fuel systems. This high-tech instrument decreases fuel consumption, thereby harmful exhaust emissions are also lowered especially in diesel ignition engines. Owing to ultra-high pressure in piezo-injection systems, fuel droplets are scaled down into a smaller particle form and thus provided more efficient combustion. Pulverized fuel droplets are evaporated and oxidized in a very short time and they provide exact combustion inside the combustion chamber. In this study, numerical simulation of a piezo-actuated common rail injector fluid-mechanical model with detail is demonstrated. The hydraulic and mechanical component interaction is modeled through the fluid-mechanical components. Thus, the piezo injector dynamics are predicted based on the geometry and the physical quantities describing the equipment. Input voltage in the entrance is used to describe the piezo actuator force for piezo-electric material. In model, fuel flows from the common rail to a tee that separates the flow into two paths: fuel gallery and valve with the inlet orifice. Using this detailed model, behavior of the piezo injector, effects of the injector parameters on the fuel flow were investigated numerically and results were represented.

Keywords: *Piezo-injector, ICE, Modeling.*

Cite this paper as: *Koten H, Gunes, EC, Guner, K. Piezo-actuated common rail injector structure and efficient design. Journal of Energy Systems 2018; 2(3): 97-114, DOI: 10.30521/jes.453560*

1. INTRODUCTION

Recently developed piezo-injectors are widely used in common rail direct injection (CRDi) systems to reduce fuel consumption and exhaust gas emissions. In Common Rail (CR) technology injection needle is directly actuated by piezoelectric mechanism, thus pilot valve usage is unnecessary, thereby a better heat release modulation during combustion and functionality required any used after-treatment instrument are obtained [1]. The direct-acting injection effect can also be obtained in solenoid CR systems by the magnetostrictive actuation system [2]. Magnetostrictive materials are able to generate effective forces without applying redundant electric current [3].

Basic benefits of direct-acting injectors may be listed as: flow-rate shaping capability, major control of the injected fuel quantity, exact and flexible multiple injections, decrease in injector leakage and very high injection pressure levels [4]. Adjustable shaping of the injected flow-rate in direct-acting piezo-injectors is provided by the accurate and flexible modulation of the time history of the current provided to the piezo-stack. Thus, unnecessary complete opening of the needle is prevented during the early injection (boot injection), which is related with keeping the seat-area smaller than the total hole area and thus controlling the injected flow-rate [5]. The definition of the boot injection parameters offers additional degrees of freedom for a more efficient management of the soot/NOx trade-off and the combustion noise [6].

The advantages of the piezo-actuated injector technology have been revealed by comparing to a solenoid type injector. The results showed that the injection delay of piezo technology was significantly shorter and the mass flow-rate enhancement during needle opening was faster [7] than in the solenoid one. The main benefits are a more efficient air–fuel mixing process and a better control of multiple injection strategies with the piezoelectric-actuated injectors than with the solenoid technology. In common-rail injection systems, the dynamic phenomena occurring such as pressure-wave propagation had been shown to be effective on the mass injected by [8] when multiple injections were used.

Injectors which use stacks of piezoelectric material as actuators have fast response times which provides capability of producing a variety of injection events [9], including rate shaping [10]. In specific, the relatively slow injection of fuel at the beginning of combustion cycle, leads to lower initial combustion temperatures, which provides for a cleaner engine with lower emissions [11].

Indirect-acting CR injectors demands for higher nozzle pressure levels (~2000 bar) [12,9], which is often restricted by the concurrent need for reduced injector leakages [13] which the fuel flow-rates that occur through the pilot valve when it is either open (dynamic leakage) or closed (static leakage). The dynamic leakage does not occur in direct-acting injectors, since there is no pilot valve, and the static leakage is lowered. Also the rail pressure can be elevated to very high levels [14] without affecting the hydraulic efficiency of the injection-system. Evidently, the no return-flow also enables the CR high-pressure pump to get minimized and removes the need for a recirculated-fuel cooler [15], in any case for injection systems controlled with fuel metering valve [16].

The common mathematical modeling of injectors can be done by an ordinary linear differential equation, as presented by Kasper et al. [17], Schernewski [18], Schugt [19] and by Raupach [20]. Wauer [21] derives a linear one-dimensional partial differential equation for piezoelectric elements. The analytical structure of some of the above mentioned analytical actuator models are appropriate to be reformulated as demodulation models that compute the mechanical values from measured electrical signals. Hereby, the model acts as a virtual sensor which may be used for a closed loop control of the actuator, as reported by Kuhnen and Janocha [22], Schugt [19] and Mehlfeldt [23]. However, demodulation models do not provide information on the entire injector mechanics. The researchers such as Schwinn and Janocha

[24], Mehlfeldt [25] and Mehlfeldt and Raupach [18] provide information for all involved mechanical parts, if an appropriate mathematical model is formed.

2. THEORY

Piezo-electric sensor or actuator part describes attributes of force electric parts, which are used to convert electrical energy into a force or to generate an electrical voltage when force or displacement is applied.

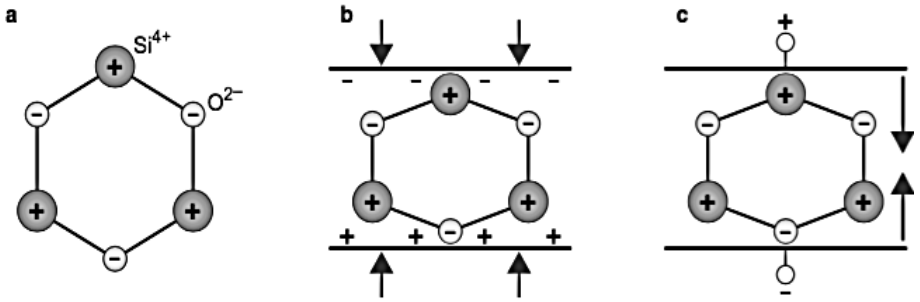

(a) Quartz crystal SiO_2, (b) Piezoelectric effect: When the crystal is compressed, negative O2– ions shift upward, positive Si^{4+} ions shift downward: Electric charges are induced at the crystal surface. (c) Inverse piezoelectric effect: By applying an electrical voltage, O^{2-} ions shift upward, Si^{4+} ions shift downward: The crystal contracts [27].

Figure 1. Schematic principle of the piezo electric effect.

The conversation of electrical to mechanical and vice versa is achieved through "piezo electric effect" of the material. Depending on the input condition the same object can be used to model a piezo actuator for a piezo sensor. In this model, it is assumed that the actuator is composed of a stack of N individual layers, each one having it thickness of 't'. It is also assumed that the dynamics of the piezo actuator from the electrical side is much faster than the dynamics from the mechanical side. In other words, the generated force F is a static function of voltage V (ideal conversion from electrical to mechanical energy) minus the spring-damper forces (k-c). This is the Force action on the mass of the piezo. When used as piezo actuator, the force generated can be calculated either using the physical properties and contractional details of the piezo element or it can be calculated using the test data of the actuator using equations below [1-3]. The force applied on the piezo mass is as follows;

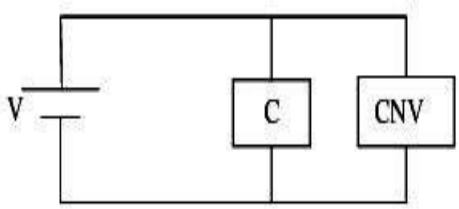

Figure 2. Piezo effect principle circuital depiction.

$$F = \phi.V - k.x - c.\dot{x} \quad (1)$$

$$F = \frac{d.E.A}{t}V - \frac{E.A}{N.t}x - c.\dot{x} \quad (2)$$

$$F = \frac{d.E.A}{t}V - \frac{E.A}{N.t}x - c.\dot{x} \quad (3)$$

Fluid piston for pressure forces and volume change part is used to model interaction between flow and mechanical systems, and is commonly used in hydraulic and pneumatic applications [26]. Specifically, this template models the following:

* Force on the attached mass due to the pressure in a chamber

* Volume Change of the chamber due to the mass displacement

2.1. Force Calculations

The force transferred to the mass is due to the pressure given as:

$$F = jP\left[\frac{\pi\left({D_p}^2 - {D_r}^2\right)}{4}\right] + F_{ext} \quad (4)$$

P : pressure in the attached flow volume

D_p : Piston Diameter

D_r : Rod Diameter

F_{ext} : External forces from any components to mechanical port

j : is based on the value of the 'Pressure Force Direction'. (If the attribute is set to "positive" j = 1, if the attribute is set to "negative" j = -1)

The flow part connected at the flow port undergoes a change in volume due to the motion of the poppet. The change in volume (ΔV) is given by the equation shown below. Note that the sign of the volume change is known based on the value of the flag Pressure Force Direction. In the equation below, j is the same as described above for the pressure force calculation (either +/- 1) [26].

$$\Delta V = j\left[\pi\frac{\left({D_p}^2 - {D_r}^2\right)}{4}\left(x - x_0\right)\right] \quad (5)$$

2.2. Linear Inertia with Upper/Lower Contacts and Friction

Simulation program models 1-D linear mass as a stop/contact in both positive and negative directions. There is also an option to model friction with multiple levels of detail, including Coulomb friction models [26]. In some cases, the contact stiffness and contact damping coefficients are not known, but rather the coefficient of restitution and contact time are known from impact experiments. Formulas are given below to convert these values to the stiffness and damping coefficients required by contacts model.

Contacts Stiffness Equations: The transition is stiffness occurs through a smooth (polynomial) curve described by the following equation;

$$K_t = K\Delta^2\ (3 - 2\Delta) \qquad (6)$$

K_t : effective contact stiffness

K : contact stiffness specified ratio of interference between two bodies *S* and Penetration for Max Stiffness S_t

Δ : δ/δ_t

The following figures show the transition of contacts stiffness and contact force for a typical metal-to-metal contact between two moving bodies (Contact Stiffness = 10^9 N/m, Stiffness Transition Layer = 10 microns)

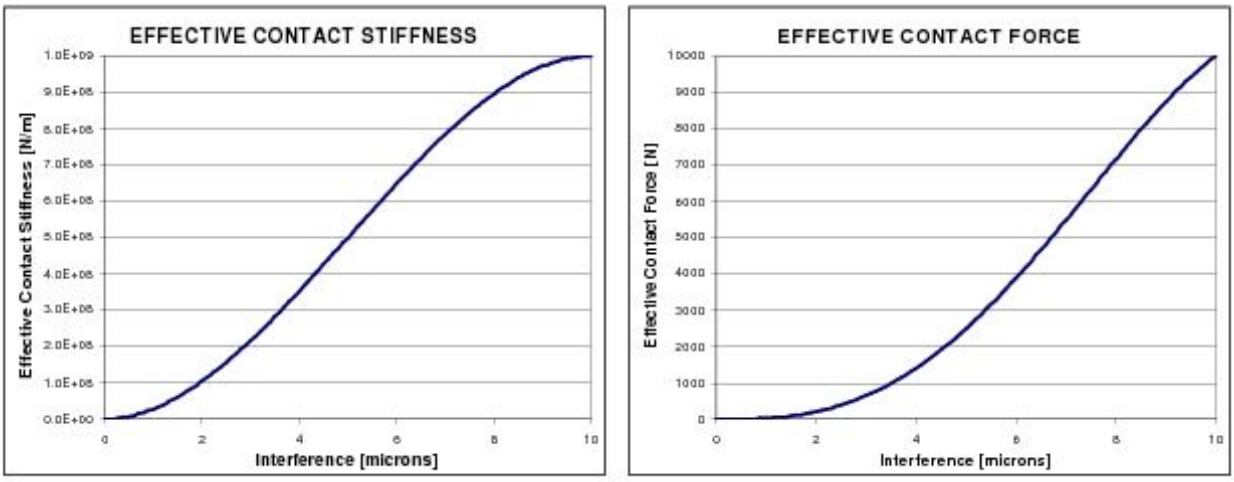

Figure 3. Effective contact stiffness [26].

2.3. Converting Coefficient of Restitution and Contacts Time to Stiffness and Damping

Sometimes it is not possible to easily determine the contacts stiffness and damping coefficient directly. One method to quantify these values is through a drop impact test, where the body is released from some height in to a solid ground. The height of the body over time is measured to give a coefficient of restitution and time of contacts. For this simple configuration of a single mass contacting a fixed ground, it is possible to convert coefficient of restitution and contact time to damping coefficient and stiffness via the formulas shown below.

$$k = \frac{m}{(\Delta T)^2}\left[\pi^2 + (lnr)^2\right] \qquad (7)$$

$$c = -\frac{m}{\Delta T} lnr \quad (8)$$

m : mass of the body

r : coefficient of restitution

c : damping coefficient

k : contact stiffness specified by the user

ΔT : time of contact

2.4. Flow Area Calculation

Ball Poppet with Conical Seat is used to model a ball poppet with a conical seat for hydraulic or pneumatic applications. The valve seat is assumed to be fixed (only the ball moves). This template calculates the change in flow area as a function of lift of the poppet, the pressure forces on the poppet, and the redistribution of volume of attached flow components due to poppet lift.

$$A_{throat} = \frac{\pi}{4}\left(D_S{}^2 - D_{rs}{}^2\right) \quad (9)$$

The area of the truncated cone between the seat and the ball valve, shown as the blue section in Figure 6, is given by:

$$A_c = \pi x_a (D_b + x_a \sin\theta) \cos\theta \sin\theta \quad (10)$$

x_a : lift of the poppet relative to seat with an upper and lower limit ($x_a = 0 \leq x \leq x_{crit}$)

D_b : ball diameter

θ : value of the attribute 'Seat Half Angle'

x_{cirit} : the lift at which the throat area equals the conical area.

$$\pi x_{crit} = (D_b + x_{crit} \sin\theta) \cos\theta \sin\theta = \frac{\pi}{4}\left(D_S{}^2 - D_{rs}{}^2\right) \quad (11)$$

2.5. Force Calculations

The total force transferred to the mass is a combination of the pressure force and the jet force:

$$F_{total} = F_{pressure} + F_{jet} + F_{ext} \quad (12)$$

F_{ext} : External forces from any components attached to the mechanical port.

The force due to pressure depends on the geometry in the following way:

If $D_{rs} > D_a$ (there is no pressure force from the seat side volume)

$$F_{pressure} = jP_2 \left[\frac{\pi\left(D_{ro}{}^2 - D_{rs}{}^2\right)}{4}\right] \quad (13)$$

otherwise:

$$F_{pressure} = j\left\{P1 \left[\frac{\pi\left(D_a{}^2 - D_{rs}{}^2\right)}{4}\right] - P2 \left[\frac{\pi\left(D_a{}^2 - D_{ro}{}^2\right)}{4}\right]\right\} \quad (14)$$

P_1 : pressure in the seat side volume

P_2 : pressure in the volume opposite the seat

D_{rs} : rod diameter (seat side)

D_{ro} : rod diameter (oppsite seat)

The jet force is calculated by the following:

$$F_{jet} = - jK_{jet}\dot{m}U\cos(\theta_{jet}) \quad (15)$$

K_{jet} : the Jet Force Multiplier as defined by the user.

U : fluid velocity

m : mass flow rate

Mass (Lumped Linear Inertia) is used to model pipes that have a round cross-section and an optional bend. Data entered to describe the bend will be used to automatically calculate the pressure loss coefficient that account for the associated head losses [26].

Double Conical Poppet with Conical Seat is used to model a conical poppet with a conical seat for hydraulic or pneumatic applications. The valves seat is assumed to be fixed (only the conical valve moves).

2.6. Flow Area Calculations

The geometrical area is calculated as a function of lift based on the following equations. The poppet lift, x, represents the gap between the valve and the seat. The formula is given below:

$$x = jx_{mass} + x_{0pos} \quad (16)$$

where is based on the value of the attribute Pressure Force Direction. If the attribute is set to “positive” j=1. If the attribute is set to “negative” j= -1.

x_{mass} : lifted of the mass attached at port 3

x_{0pos} : lift at zero position (can be used to account for a non-zero gap between the poppet and the seat when the mass attached at port 3 is at zero position)

The geometrical area is always limited to the minimum of the throat area, the two conical areas, the upstream flow part area (A_{up}), and the downstream flow part area (A_{down}).

$$min\ (A_1,A_2) - A_{throat} = 0 \tag{17}$$

As this equation may have several solutions in the interval the root is determined for lift in the following interval:

$$10^{-20} \leq x \leq \frac{D_s}{sin(max(\alpha,\sigma))} \tag{18}$$

D_s : Diameter of Hole

σ : Needle Cone Half Angle

α : Seat Half Angle

The value of the transition lift script can be found as RLT in the main folder. So the geometrical area A_g is defined by:

$$If, \quad x \leq xcrit \quad A_g = min\ (A_1, A_2, A_{throat}, A_{up}, A_{down}) \tag{19}$$

$$If, \quad x > x_{crit} \quad A_g = min\ (A_{throat}, A_{up}, A_{down}) \tag{20}$$

where,

$$A_{throat} = \pi/4(D_s{}^2 2 - D_r{}^2) \tag{21}$$

D_s : Diameter of Hole

D_r : Diameter of Rod (seat side)

The area available for flow A_{flow} is calculated by the following:

$$A_{flow} = C_d A_g \tag{22}$$

2.7. Discharge Coefficient Calculations

Based on experimental measurement data provided in many fluid power books, the discharge coefficient through hydraulic valves can be represent by the equation shown below.

$$\lambda = \frac{D_h}{v}\sqrt{\frac{2}{\rho}|P_2 - P_1|} \tag{23}$$

Where λ is the flow number and λ_{crit} is the Critical Flow Number. Note that at $\lambda=\lambda_{crit}$, $C_d = 0.964C_{d,max}$ and $\lambda = 2\ \lambda_{crit}$, $C_d=0.9993C_{d,max}$ .The flow number is similar to the Reynolds number expect that the velocity is replaced with the isentropic velocity. This is done to eliminate an algebraic loop that would occur since otherwise $C_d = f(v)$ and $v= f(C_d)$.

The hydraulic diameter, needed to calculate the flow number, and thus C_d, is calculated in a simplified manner for this complex valve.

$$C_d = C_{d,max}\ tanh\left(\frac{2\lambda}{\lambda_{crit}}\right) \tag{24}$$

$$D_h = \frac{4A_{flow}}{P_{wet}} = 2xsin\alpha \tag{25}$$

where P_{wet} is the wetted perimeter [26].

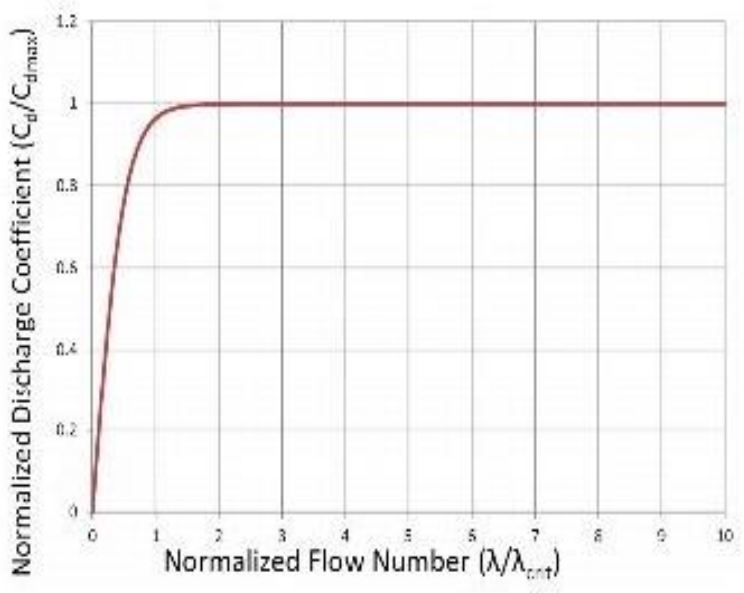

Figure 4. Discharge coefficient versus normalized flow number [26].

3. METHODOLOGY and MODEL

In this numerical study, piezoinjector components were modeled and linked each other to analyze the behavior of injector. All parts of piezoinjector were modeled and analyzed numerically. In literature, some investigations were made to analyze the behavior of piezoinjector [1-4]. In this study, in the Signal Generator part, the injector output phase is triggered by ECU particularly designed for piezo injectors. A reference trigger voltage is predetermined as a function of the rail pressure of the defined operating point. The output voltage in the model is produced using the "Signal Generator" part. Thus, it is aimed to convert the voltage increase proportionally into a piezoelectric actuator pulse [27]. Designed for a high-performance diesel engine, the piezo injector is simulated with the thermodynamic equations. Templates used in the program are shown in Figure 5.

3.1. Nozzle Holes of Detailed Predictive Injector Model

It was defined in a detailed, predictive injector model where all the injector flow volumes, mechanics and hydro-mechanical interaction are considered.

Nozzle Discharge Coefficient Model: Name of a discharge coefficient model reference object used to define the nozzle discharge coefficient. This reference object can be a cavitating model or a user-imposed value.

Reference Pressure (for Volume Flow Rate output only): A reference pressure used to calculate density convert from mass flow rate to volume flow rate. Numerical code solves the governing equations to obtain mass flow rate. To convert to volume flow rate, an appropriate reference fluid density must be obtained based on the pressure and temperature of the fluid. For many injection system measurements, the fluid density is taken at a reference pressure of 1 bar, which is the "def" value for this attribute. A value of "ign" may be entered to specify the upstream pressure. This attribute must be used in conjunction with Reference Temperature [26].

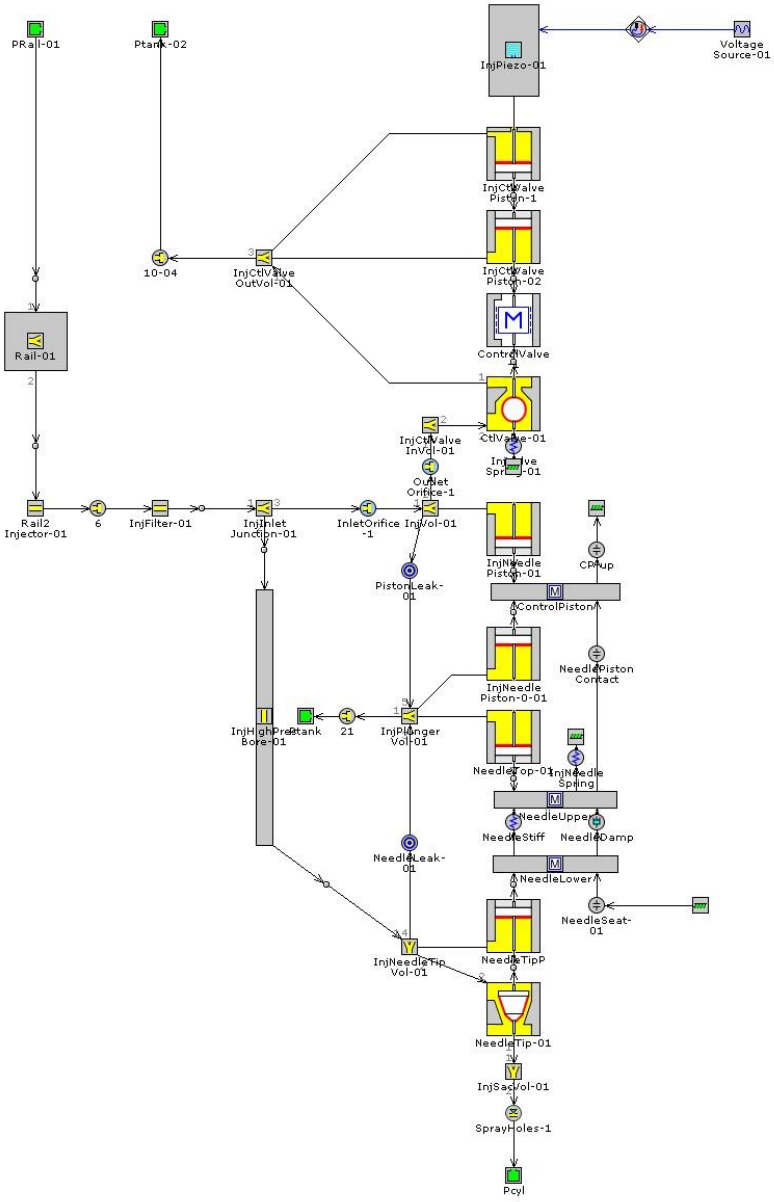

Figure 5. Piezo injector model [26].

Reference Temperature (for Volume Flow Rate output only): A reference pressure used to calculate density convert from mass flow rate to volume flow rate. Numerical code solves the governing equations to obtain mass flow rate. To convert to volume flow rate, an appropriate reference fluid density must be obtained based on the pressure and temperature of the fluid. If comparing to measured data, this temperature may correspond to the temperature of the fluid at the location where volume flow rate is measured on your test bench. Whenever comparing volume flow rates to any other source, please pay careful attention to the volume flow rates are reported to make sure they are consistent a value of "ign" may be entered to specify the upstream temperature. This attribute must be used in congestion with Reference Pressure [26].

Reference Fluid Object (for Volume Flow Rate output only): A reference fluid object used to calculate density to convert from mass flow rate to volume flow rate. Numerical code solves the governing equations to obtain mass flow rate. To convert to volume flow rate, an appropriate reference fluid density must be obtained based on the pressure and temperature of the fluid. A value of "def" specifies the upstream fluid. A value other than "def" is typically not recommended.

One example where this attribute could be used is for a liquid system with a large fraction of gas cavitation vapor but the physical measurement device treats the entire volume as liquid [26].

"End Environment part" describes end environment boundary conditions of pressure, temperature and composition.

"Flow Volume with General Geometry" is used to describe a flow-split volume connected to one or more flow components. This object can be used to describe any shape of flow-split.

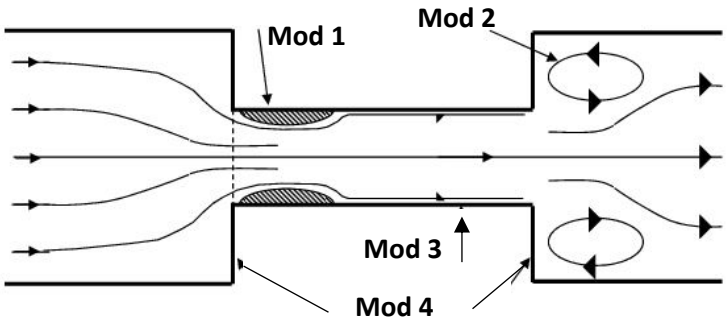

Figure 6. Orifices [26].

"Orifices between two flows components" describe an orifice placed between any flow components 'OrificeConn' parts represent the plane connecting two flow components. The momentum equation, as shown in the Flow Manual, is solved to calculate the flow rate through the orifice [26].

3.2. Pressure Loss Modes in the Orifice

There are several modes of pressure loss that can happen in the OrficeConn illustrates these forms of loss, which include;

a) loss due to contraction,
b) loss due to expansion,
c) loss due to hole thickness friction and
d) loss due to friction.

Loss Mode 1: At discontinuous contractions, velocity toward the center results in a vena contract and contraction loss. The Cd characterizes the vena contract. Cd= def assumes discontinuity.

Loss Mode 2: At discontinuous expansions, velocity becomes a turbulent eddy and kinetic energy is turned into heat via internal and surface friction. Expansion loss does not occur in the throat though.

Effective Area= Geometric Area, Cd=def=1.0

Loss Mode 3: Friction along the thickness of the orifice

Loss Mode 4: Friction along the face of the orifice when flow is laminar.

Leakage Annular: Annular Leakage Connection is used to model the laminar leakage flow past a cylinder (e.g. piston or plunger) in a guide, sleeve, or barrel where the clearance is much smaller than the diameter of the piston. The model takes into account the pressure differential across the element and the effect of the relative motion of the rod with respect to the guide (Poiseuille and Couette flow) [26, 30, 31].

Leakage volumetric flow rate is calculated using a Poiseuille/Couette flow solution for flow between parallel plates, and thus is only valid when $\delta << D$

$$Q = M\left[\pi D\delta\left(\frac{\delta^2\Delta p}{12\,\mu L}\right) + \frac{1}{2}\,U_{wall}\right] \qquad (26)$$

D : diameter of the annulus

Q : volume flow rate

δ : thickness of annular passage

Δp : pressure differential

μ : dynamic viscosity calculated at

P : upstream pressure

T : temperature for viscosity calculation

L : length of annular passage

U_{wall} : relative velocity between piston and bore

M : flow rate multiplier

"Round Pipe with Bend" is used to model pipes that have a round cross-section and an optional bend. Data entered to describe the bend will be used to automatically calculate the pressure loss coefficient that account for the associated head losses. The "AF Ratio" and "λ" sensors give the reconstituted air-to-fuel ratio and lambda value of all chemical species present in the system. All species containing C, H, O, or S are detected the sensor location. The amount of C, H, and S atoms are counted and necessary oxygen to get H_2O, CO_2 and SO_2 as a product is determined. The "λ" sensor is defined as (total oxygen atoms) / (total oxygen atoms required to oxidize all carbon, hydrogen, and sulfur atoms) [26].

Lambda calculation example:

Mixture composition;

$$\alpha\, CO_2 + \beta\, CO + \delta\, H_2O + \varepsilon\, C_x H_y \tag{27}$$

$$C: \alpha + \beta + \varepsilon.\, x \tag{28}$$

$$H: 2.\, \delta + \varepsilon.\, y \tag{29}$$

$$O_2{}^{mixture} : \alpha + \frac{\delta}{2} + \frac{\beta}{2} \tag{30}$$

Stoichiometric Oxygen;

$$C_{\alpha+\beta+\varepsilon.x} + H_{2.\delta+\varepsilon.y} + O_2{}^{stoich} = m\,.\,CO_2 + n\,.\,H_2O \tag{31}$$

$$O_2{}^{stoich} : \alpha + \beta + \varepsilon\,.\,x + \frac{2\delta + \varepsilon\,.\,y}{4} \tag{32}$$

Lambda:

$$\lambda = \frac{O_2{}^{mixture}}{O_2{}^{stoich}} \tag{33}$$

The "λ_{old}" sensor is similar to the "λ" sensor, but disregards any fuel-bound oxygen in the system.

Following the above example:

$$O_2{}^{fuel} : \frac{\beta}{2} \tag{34}$$

$$\lambda_{old} = \frac{O_2{}^{mixture} - O_2{}^{fuel}}{O_2{}^{stoich} - O_2{}^{fuel}} \tag{35}$$

Orifice with cavitation between two flow components are used to model an orifice between any two components where cavitation may occur. The discharge coefficient can be modelled in a number of ways with discharge coefficient reference objects, including a model based on a critical cavitation number or a predictive model based on the orifice geometry.

Actuate/ Pilot a Value in Multi-Physics Templates are a link between controls library and multi-physics library (i.e. flow, mechanical, thermal etc.). 1-D Contacts (gap) with Stiffness and Damping represent 1-dimesional contact between two mechanical bodies. The total contact force is a result of both stiffness and damping components. This part applies on the two parts attached to the 'Contact' connection when the gap (calculated from the relative motion of the two connected parts) becomes less than zero. The forces on the two parts will be of opposite sign, and the direction of the linking arrow will determine the

direction of the force discussed below under the heading “Calculation of Contact Force” section [26, 32, 33].

Spring - Massless Spring Connection part is a massless standard spring that can be used to connect component parts with transitional degrees of freedom. Attributes of the ‘Spring’ part are as a follow:

Stiffness: Spring stiffness used to calculate the force. Entering “def” causes the spring stiffness to be set to 0 N/m.

Preload: Spring preload force when the position of both part is zero. To determine whether a positive or negative value should be entered, please see the equations below. Entering “def” causes the pretension to be set to 0 N.

Ground with Zero or Known Position part describes the attributes of ground parts used to specify a fixed node with known position or angle.

4. RESULTS and DISCUSSIONS

The graphics we obtained from commercial injector modelling and analysis program show that poppet lift of injector occurs in nearly 1 millisecond. In Figure 7 it can be seen that poppet lifts about 0.22 mm and reaches maximum velocity of nearly 875 m/s at the closing. The velocity of the poppet first reaches about 400 m/s at the opening and decreases instantly afterwards and then reaches a peak value when closing. The instant increase in velocity at the closing minimizes fuel leakage in the orifices.

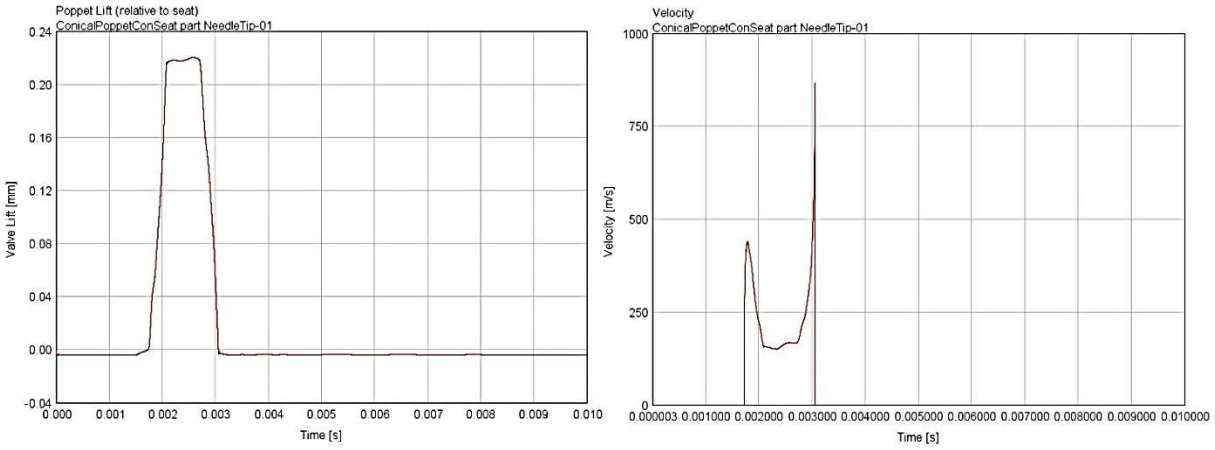

Figure 7. Poppet lift and velocity variation with time during injection

Volumetric and mass flow rates of fuel during injection can be seen in Figure 8. The regime of both are expected to be same since there is not a significant change in the density of fuel during injection. Mass flow rate reaches about 0.055 kg/s peak value in the middle of injection time, and volumetric flow rate reaches the peak value of 0.0625 L/s at the same time step.

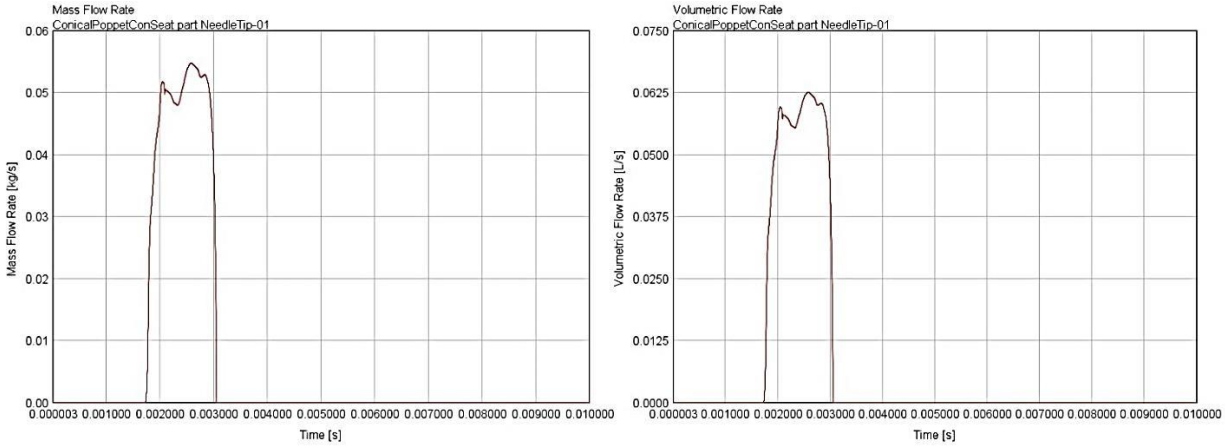

Figure 8. Mass and Volumetric flow rates values during injection

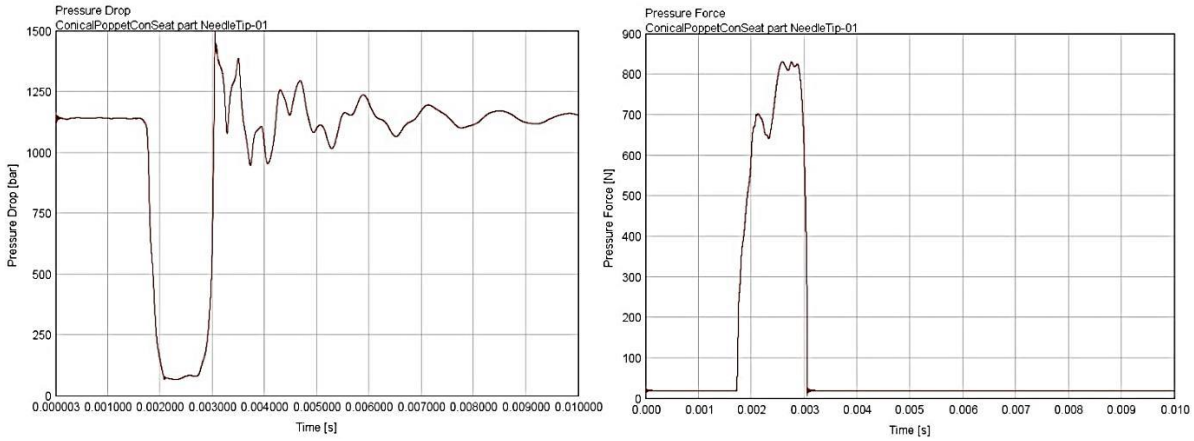

Figure 9. Pressure Drop and Pressure Force values during injection

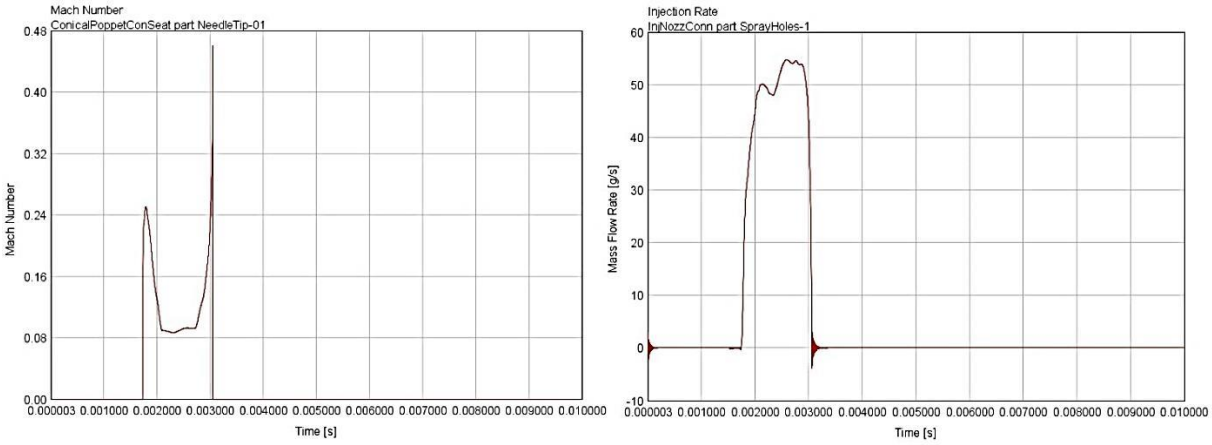

Figure 10. Mach Number and injection rate values during injection

5. CONCLUSION

Piezo-injectors are high-tech equipment widely used in internal combustion engines' common rail fuel system. They operate in ultra-high pressures which provides fuel to become fully atomized and mixed with air efficiently. Thus, fuel consumption and emissions are lowered. Piezo injectors work on the principle of electrical/mechanical pulse conversion. In this study, zero dimensional software was used to model and analyze of the piezo-injector components. At the study, piezo-injector components were separately modeled part by part and linked each other to analyze the behavior of injector.

Equations of mathematical model are given in theory section. All parts of a piezo-injector were modeled and analyzed numerically based on these equations. Poppet lift distance and velocity, mass/volumetric flow rate of fuel during injection, pressure drop and pressure force, Mach number and injection rate values are obtained from analysis results. Results were consistent with analytical values and expected flow behaviors. Injection cycle happens in nearly 1 millisecond and poppet's movement and velocity forms in this interval. The poppet lifts about 0.22 mm and reaches 875 m/s of maximum velocity at the opening and closing phase. Maximum velocity occurs in closing movement of poppet. This is caused by fuel flow behavior, also provides fuel leakage to be minimum. Mass and volumetric flow rates has maximum values of 0.055 kg/s and 0.0625 L/s respectively, which proves to be fuel's density nearly 0,88 kg/L.

In conclusion, piezo-injector is an efficient equipment widely used today's automotive industry. They can provide fast and precise injection of fuel in a very short time interval. Owing to piezoelectric mechanism, opening and closing of poppet happens quite fast which optimizes fuel injection and atomization. Injection parameters can be obtained from a commercial software which utilizes mathematical equations and numerical approaches. This helps end-users make their designs more efficient and optimized.

Acknowledgement

This study is part of the developing of clean diesel engine design project supported by TUBITAK 2219 programme.

REFERENCES

[1] Bauer S, Zhang H, Pfeifer A, Wenzlawski K. Diesel engines for passenger cars and Euro 6: entire system approach for the development of the fuel injection system, the air/EGR path and the emission after-treatment. In: 28th International Vienna Motor Symposium, 26-27 April 2007, Fortschritt-Berichte VDI, Reihe 12: Verkehrstechnik/Fahrzeugtechnik, Vienna: pp. 265-285

[2] Tanaka H, Sato Y, Uri T. Development of a Common-Rail proportional injector controlled by a tandem arrayed giant-magnetostrictive-actuator. SAE Technical Paper 2001-01-3182 <https://doi.org/10.4271/2001-01-3182>

[3] Bright CB, Garza JC. Possible very high speed rate shaping fuel injector. SAE Technical Paper 2007-01-4113 <https://doi.org/10.4271/2007-01-4113.>

[4] Delphi Automotive. Direct acting light-duty diesel CR system. 2008, Technical Report.

[5] Tanabe K, Kohketsu S, Nakayama S. Effect of fuel injection rate control on reduction of emissions and fuel consumption in heavy duty DI Diesel engine. SAE Technical Paper 2005-01-0907 <https://doi.org/10.4271/2005-01-0907>

[6] Atzler F, Kastner O, Rotondi R, Weigand A. Multiple injection and rate shaping. Part 1: Emission reduction in passenger car diesel engines. SAE Technical Paper 2009-24-0004 <https://doi.org/10.4271/2009-24-0004>

[7] Payri R, Salvador FJ, Gimeno J, De la Morena J. Influence of injector technology on injection and combustion development – Part 1: hydraulic characterization. Appl Energy 2011; 88:1068–74. <https://doi.org/10.1016/j.apenergy.2010.10.012>
[8] Catania AE, Ferrari A, Manno M, Spessa E. Experimental investigation of dynamics effects on multiple-injection common rail system performance. J Eng Gas Turbines Power 2008; 130:032806-2 <https://doi.org/10.1115/1.2835353>
[9] Payri, R., Salvador, F., Gimeno, J., & la Morena, J.D. Influence of injector technology on injection and combustion development—Part 1: Hydraulic characterization. Applied Energy 2011, 1068–1074 <httpps://doi.org/10.1016/j.apenergy.2010.10.004>
[10] MacLachlan, B., Elvin, N., Blaurock, C., & Kegan, N. Piezoelectric valve actuator for flexible diesel operation. In: Smart Structures and Materials, 14-18 March 2004, Industrial and commercial applications of smart structures technologies, San Diego, California, USA: pp. 167-178.
[11] Wakisha, Y., Azetsu, A., & Oikawa, C. Effect of fuel injection rate shaping on spray combustion—Effect of the slope of injection rate rise on combustion. In University of Tokyo 4th COMODIA symposium, 1998 (pp. 441–446).
[12] Boecking F. Passenger car CR systems for future emission standards. In: MTZ 7-8/2005, 2005, pp. 552–557.
[13] Catania AE, Ferrari A, Mittica A, Spessa E. Engine performance comparison between different last generation typologies of advanced piezo and solenoid fuel injection systems. Commissioned technical report, Politecnico di Torino, Torino; November 2009.
[14] Kastner O, Atzler F, Juvenelle C, Rotondi R, Weigand A. Directly actuated piezoinjectors for advanced injection strategies towards cleaner diesel engines. In: 7th Int. symposium towards cleaner diesel engine TDCE 2009, Aachen, June 2009.
[15] Delphi Automotive. Direct acting light-duty diesel CR system. Technical report; 2008.
[16] Catania AE, Ferrari A. Experimental analysis, modeling and control of volumetric radial-piston pumps. ASME Trans, J Fluids Eng 2011;133(8):081103 < https://doi.org/10.1115/1.4004443>
[17] Kasper R, Schröder J, Wagner A. Schnellschaltendes hydraulikventil mit piezoelektrischem stellantrieb. O¨ lhydraul Pneumat 1997; 41:694–8.
[18] Schernewski R. Modellbasierte Regelung ausgewahlter Antriebssystemkomponenten im Kraftfahrzeug. PhD thesis, Universitat Fridericiana zu Karlsruhe, Germany, 1999.
[19] Schugt M. Aktor-Sensorverhalten von Piezoelementen in Kfz-Diesel-Einspritzsystemen. PhD thesis, Ruhr-Universitat Bochum, Germany, 2001.
[20] Raupach C. Verfahren zur Stabilisierung der Kraftstoffdosierung bei Piezo-Einspritzventilen. PhD thesis, Ruhr-Universitat Bochum, Germany, 2007.
[21] Wauer J. Zur modellierung piezoelektrischer wandler mit verteilten parametern. Z Angew Math Mech 1997; 77:365–6.
[22] Kuhnen K, Janocha H. Nutzung der inharenten sensorischen eigenschaften von piezoelektrischen aktoren. Tech Messen 1999, 66(4):132–8.
[23] Mehlfeldt D. Modellierung und optimale Steuerung piezoelektrisch aktuierter Einspritzventile. PhD thesis, Universitat Siegen, Germany, 2006.
[24] Schwinn A, Janocha H. Self-configurable actuator–sensor-array for active vibration suppression. München 2000. Materials week.
[25] Mehlfeldt D, Raupach C. Possibilities and limits of the utilization of inherent sensor properties of piezoelectric actuators. Berlin, 2007. Steuerungssysteme für den Antriebsstrang von Krtaftfahrzeugen.
[26] Koten H. Piezo-Actuated Common Rail Injector Structure and Efficient Design, 6th Eur. Conf. Ren. Energy Sys. 25-27 June 2018, Istanbul, Turkey.
[27] Konrad, R. Diesel Engine Management, BOSCH, 2014.
[28] Parthasarathy, M, Joshua Ramesh Lalvani, I, Dhinesh, B, Annamalai, K. Effect of hydrogen on ethanol–biodiesel blendon performance and emission characteristics of a direct injection diesel engine, ELSEVIER, Ecotoxicology and Environmental Safety 2016, 134:433–439 <https://doi.org/10.1016/j.ecoenv.2015.11.005>
[29] Nalgundwar, A., Paul, B., Sharma, S., "Comparison of performance and emissions characteristics of DI CI engine fueled with dual biodiesel blends of palm and jatropha", 2016. ELSEVIER, Fuel 173, 172–179 <httpps://doi.org/10.1016/j.fuel.2016.01.022>
[30] Viera, J. P., Payri, R., Swantek, A. B., Duke, D. J., Sovis, N., Kastengren, A. L., Powell C. F., 2016. "Linking instantaneous rate of injection to X-ray needle lift measurements for a direct-acting piezoelectric injector", ELSEVIER, Energy Conversion and Management 112, 350–358 <https://doi.org/10.1016/j.enconman.2016.01.038>
[31] Nouraei, H. Design and Development of a Direct-Acting Piezoelectric Fuel Injector (MSc)., Department of Mechanical and Industrial Engineering University of Toronto, Canada, 2012.

[32] Pogulyaev, Y.D., Baitimerov, R.M., Rozhdestvenskii, Y.V. Detailed Dynamic Modeling of Common Rail Piezo-Injector, Procedia Engineering 2015, 129:93-98 <https://doi.org/10.1016/j.proeng.2015.12.014>

[33] Payri, R., Salvador, F.J., Carreres, M., De la Morena, J. Fuel temperature influence on the performance of a last generation common-rail diesel ballistic injector. Part II: 1D model development, validation and analysis, Energy Conversion and Management 2016, 114:376-391 <https://doi.org/10.1016/j.enconman.2016.02.043>